Half-metallic antiferromagnetic nature of La_2VTcO_6 and La_2VCuO_6 from *ab initio* calculations

Y. K. Wang,[1,*] P. H. Lee,[2] and G. Y. Guo[3,4,†]

[1]*Center for General Education and Department of Physics, National Taiwan Normal University, Taipei 106, Taiwan*

[2]*The Affiliated Senior High School of National Taiwan Normal University, Taipei 106, Taiwan*

[3]*Graduate Institute of Applied Physics, National Chengchi University, Taipei 116, Taiwan*

[4]*Department of Physics, National Taiwan University, Taipei 106, Taiwan*

(Received 27 August 2009; revised manuscript received 23 November 2009; published 17 December 2009)

Electronic structure calculations based on density-functional theory with the generalized gradient approximation for 406 double perovskites $La_2BB'O_6$ have been performed using the accurate full-potential linearized augmented plane wave method. La_2VTcO_6 and La_2VCuO_6 are found to be candidates of half-metallic (HM) antiferromagnets (AFM) among the 406 ordered double perovskites $La_2BB'O_6$ with all the possible B and B' pairs from all the 3*d*, 4*d*, and 5*d* transition metals have been considered. Furthermore, the HM-AFM state in La_2VTcO_6 and La_2VCuO_6 survive the full lattice constant and atomic position optimizations which were carried out using the frozen-core full-potential projector-augmented wave method. In addition, the GGA+U electronic structure calculations have also been performed and the HM-AFM state still remains. Their AFM state is attributed to both the superexchange and generalized double exchange mechanisms via the $B(t_{2g})$-$O(2p_\pi)$-$B'(t_{2g})$ coupling, and the latter could also be the origin of their HM.

DOI: 10.1103/PhysRevB.80.224418 PACS number(s): 75.10.Lp, 71.20.−b, 75.30.−m, 75.50.Ee

I. INTRODUCTION

Based on the band structure calculations for magnetic semi-Heusler compounds NiMnSb and PtMnSb, the concept of half-metallic (HM) ferromagnets (FM) was first discovered by de Groot *et al.*[1] After this important discovery, half-metallic ferromagnets (HMFs) immediately attracted much research for their potential applications in spintronics and novel fundamental physics.[2–4] Typical examples of HM magnetic materials include spinel Fe_3O_4,[5] rutile CrO_2,[6] mixed-valence perovskite $La_{0.7}Sr_{0.3}MnO_3$,[7] double perovskite Sr_2FeMoO_6, and Sr_2FeReO_6,[3,8] spinel $FeCr_2S_4$,[9] and Mn-doping GaAs.[10,11] Half-metallic materials are characterized by the coexistence of metallic behavior in one electron spin channel followed by insulating behavior in the other. Their electronic density of states is completely spin polarized at the Fermi level, and conductivity is dominated by these metallic single-spin charge carriers. Therefore, half-metallic materials offer potential technological applications in the realm of single-spin electron source and high-efficiency magnetic sensors.[2–11]

In a HM material, due to a band gap at Fermi energy (E_F) for one spin channel, the spin magnetic moment per unit cell is quantized, i.e., an integer number times Bohr magneton (μ_B).[1–4,7–9] Apart from a ferromagnetic (FM) state with parallel atomic spin arrangements, an antiferromagnetic (AFM) state, in which different atomic spins are aligned antiparallel, is another possibility. In the AFM state, the net moment per unit cell must be zero if the material possesses the properties of HM and AFM. Clearly, in a HM-AFM, there are at least two different ions with their spins being antiparallel and hence canceling each other exactly.

The first concept for a HM-AFM was proposed by van Leuken and de Groot.[12] They predicted theoretically that the Heusler compound, $V_7MnFe_8Sb_7$, was a HM-AFM. Most properties such as full spin-polarized conduction electrons, zero spin susceptibility, and non-Stoner continuum of these HM-AFMs are the same as those of the HM-FMs discussed above.[4] However, a crucial difference is that a HM-AFM produces no macroscopic magnetic field. By utilizing this kind of materials, one would be able to develop a probe of the spin-polarized scanning tunneling microscope without perturbing the spin character of samples.

Recently, several theoretically predicted HM-AFM candidates have attracted considerable attention because of the valuable potential of their future applications. They include the half-Heusler[12] and full-Heusler alloys,[13,14] double perovskites,[15–18] and thiospinels.[19] Other possible candidates include disordered systems such as vacancy-induced rocksalt transition metal oxides,[20] Co-substituted Heusler alloys,[21] and diluted antiferromagnetic semiconductors.[22,23] Furthermore, Pickett[24] proposed to use HM-AFMs as a base for a new type of superconductor with just one superconducting spin channel—the so-called single-spin superconductor. HM-AFMs are expected to play a vital role in future spintronic devices that utilize the spin polarization of carriers. Unfortunately, in spite of many theoretical predictions, to date, none of the proposed HM-AFMs has been verified experimentally.

It is conceivable that a HM-AFM could support 100% spin-polarized charge transport without any net magnetization. Because of the spin-rotational symmetry and equivalence, the conventional AFMs, such as bcc Cr, cannot be half-metallic. Other possible choices for suitable HM-AFMs are ferrimagnets with a compensated magnetic moment. The simplest solution, however, is to develop a material in which the unit cell is composed of two different magnetic ions whose moments are equal in magnitude but antialigned. With this in mind, there is one obvious choice for the HM material: double perovskite Sr_2FeMoO_6 in the ferrimagnetic state with the Fe spin moment being higher than that of Mo. It is possible to design a double perovskite HM-AFM by choosing a proper pair of transition metal ions with their magnetic moments cancelling out exactly.

Compared with the complex Heusler compound $V_7MnFe_8Sb_7In$ (Ref. 12), there are several good reasons why

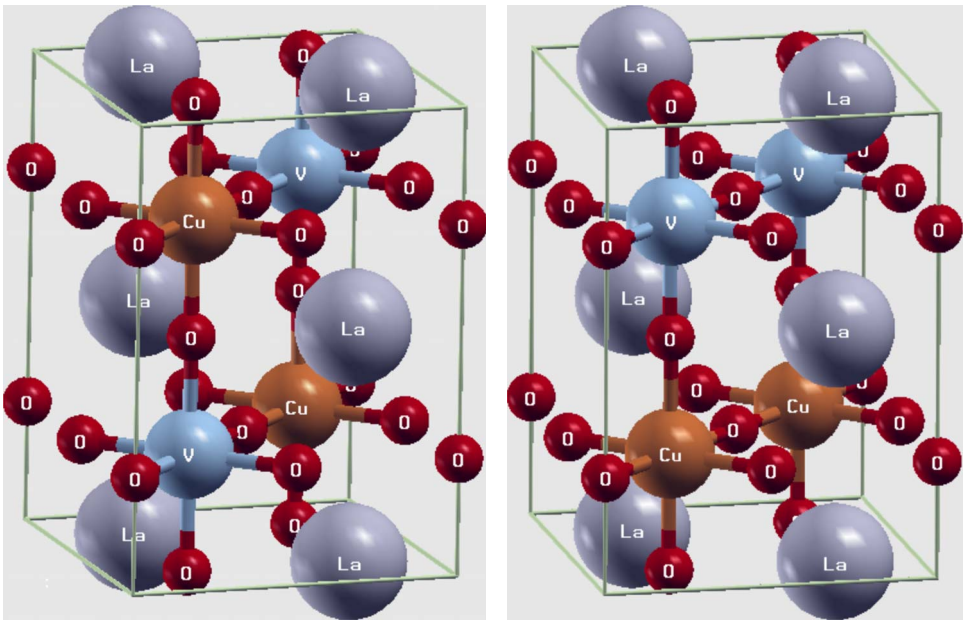

(a) (b)

FIG. 1. (Color online) The double perovskite crystal structure. (a) Cubic $Fm\bar{3}m$ [111] stacked structure and (b) tetragonal $P4/mmm$ [001] stacked structure

the double perovskites would be a better system to search for the HM-AFM. First, the number of double perovskite candidates is very large. Second, the relatively simpler crystal structure embodies the possibility for the two different magnetic ions encompassed within the similar environments to cancel out their moments exactly. Another important fact is that the double perovskites are easy to synthesize. This leads to the primary purpose of the present paper which is to search for the HM-AFM candidates from the double perovskites by first-principles density-functional calculations. In fact, Pickett[15] suggested earlier to use the double perovskite structures instead of the Heusler alloys as possible candidates, and also predicted La_2VMnO_6 as a specifically suitable candidate. Furthermore, double perovskites $LaAVRuO_6$,[16] $LaAVMoO_6$,[18] $LaAVOsO_6$, and $LaAMoYO_6$ (Ref. 17) (A=Ca, Sr, and Ba and Y=Re and Tc) have been postulated as possible HM-AFMs, thus showing the double perovskites to be a fertile class of candidates for this new type of HM-AFMs.

In this paper, in order to search for new HM-AFMs from double perovskite oxides $La_2BB'O_6$, we have thoroughly explored a variety of pairs BB' with B and B' from all 3d (Sc, Ti, V, Cr, Mn, Fe, Co, Ni, Cu, Zn), 4d (Y, Zr, Nb, Mo, Tc, Ru, Rh, Pd, Ag, Cd), and 5d (Hf, Ta, W, Re, Os, Ir, Pt, Au, Hg) transition metals except La, i.e., we have studied a total of C_2^{29} or 406 possible combinations of $La_2BB'O_6$ compounds. After a large number of calculations, we find the La_2VTcO_6 and La_2VCuO_6 are suitable candidates for HM and AFM materials. Furthermore, for these two cases, we not only carried out full structural optimizations but also considered the possibilities of $LaBO_3/LaB'O_3$ ordered in both the cubic $Fm\bar{3}m$ [111] stacked structure [Fig. 1(a)] and tetragonal $P4/mmm$ [001] stacked structure [Fig. 1(b)]. Finally, we find that La_2VTcO_6 in the [111] stacked structure a robust and stable HM-AFM, while it in the [001] stacked structure is a metastable FiM metal. We also find that the energy of La_2VCuO_6 with the [111] stacked structure is higher than that in the [001] stacked structure, i.e., La_2VCuO_6 in the [111] stacked structure is a metastable HM-AFM.

The rest of this paper is organized as follows. In the next section, we introduce their crystalline structures as well as the details of theoretical computations. In Sec. III, we discuss the calculated structural stability as well as electronic and magnetic properties. Finally, in Sec. IV, we summarize our findings.

II. CRYSTAL STRUCTURE AND COMPUTATIONAL DETAILS

We considered $La_2BB'O_6$ in an ordered double perovskite structure (space group $Fm\bar{3}m$) in which B and B' form the NaCl-type lattice (face centered cubic), [111] stacked structure as shown in Fig. 1(a). This structure can be regarded as a combination of BO_3 and $B'O_3$ octahedra in a superlattice having B and B' layers stacked along the [111] direction, as exemplified by La_2CrFeO_6 and Sr_2FeMoO_6.[3,25] Each $B(B')$ ion has six $B'(B)$ neighbors. BO_3 and $B'O_3$ octahedra can also be stacked along the [001] direction, resulting in the tetragonal structure with the space group $P4/mmm$ with $c=2a$, as shown in Fig. 1(b). In this case, each B ion has four B ions and two B' ion neighbors, and vice versa. In both [111] stacked and [001] stacked structures, we considered both the ferromagnetic and antiferromagnetic states. Both ideal cubic $Fm\bar{3}m$ structure and tetragonal $P4/mmm$ structure contain 10 atoms per unit cell, i.e., one chemical formula unit (f.u.).

Our theoretical search was based on first-principles calculations within density-functional theory (DFT) (Ref. 26) with the generalized gradient approximation (GGA) to the exchange-correlation potential.[27] To determine theoretical lattice constants and atomic positions by structural optimization calculations, however, we considered a larger unit cell with 2 f.u. because we wanted to allow the structure relax to

a reduced symmetry. Indeed, after full structural optimization (i.e., relaxation of both lattice constants and atomic positions), the $Fm\bar{3}m$ structures could be reduced to the $I4/mmm$ structure, while the $P4/mmm$ structure remained unchanged. These structural optimizations were carried out using the faster frozen-core full-potential projector-augmented wave (PAW) method[28] as implemented in the VASP package.[29] A cutoff energy of 450 eV for plane waves was used. An $8\times8\times6$ Monkhorst-Pack k-point grid in the Brillouin zone was used, which corresponds to 30 k points in the irreducible Brillouin-zone wedge. Their atomic positions and lattice constants were fully relaxed by a conjugated gradient technique. The energy convergence criterion was set to 10^{-5} eV. Theoretical equilibrium structures were obtained when the forces and stresses acting on all the atoms were less than 0.01 eV/Å and 1.2 kBar, respectively.

Before and after the structural optimizations by the PAW method, we used the highly accurate full-potential linearized augmented plane wave (FLAPW) method[30,31] as implemented in the WIEN2K package,[32] to calculate the total energy, electronic structure and magnetic properties of the perovskites with the structural parameters fixed. The wave function, charge density, and potential were expanded in terms of the spherical harmonics inside the muffin-tin spheres. The cutoff angular momentum (L_{max}) of 10 used for the wave function, and of 6 used for the charge density and potential, are sufficient for accurate total-energy and electronic structure calculations. The wave function outside the muffin-tin spheres was expanded in terms of the augmented plane waves. A large number of augmented plane waves (about 120 per atom, i.e., $R_{mt}K_{max}=6$) were included in the present calculations. The set of basis functions was supplemented with local orbitals for additional flexibility in representing the valence V and Cu $3d$ states, Tc $4d$ states, and La $4f$ and $5d$ states, as well as for the semicore La $5s$, $5p$, O $2s$ states. The muffin-tin sphere radii used were 2.5 a.u. for La, 2.0 a.u. for V, Cu, and Tc, and 1.4 a.u. for O. The improved tetrahedron method is used for the Brillouin-zone integration.[33] The numbers of k points in the irreducible Brillouin-zone wedge used were 120, 163 and 180 for the $Fm\bar{3}m$, $I4/mmm$, and $P4/mmm$ structures, respectively.

We note that the electronic structure of a system with strong electron correlation, such as transition metal oxides, is often not well described by DFT-LDA(GGA) calculations. Currently, this deficiency in first-principles electronic band structure calculation is corrected by including an on-site Coulomb interaction correction to the LDA or GGA, the so-called LDA(GGA)+U method.[34,35] This LDA(GGA)+U scheme, yielding quite satisfactory results for many strongly correlated systems is considered to be an useful approach.[36–38] Therefore, to see the effects of the on-site electron correlations on the half-metallicity and magnetic properties of the materials considered, we also performed the GGA+U calculations for the found HM-AFMs.

III. RESULTS AND DISCUSSION

A. Found half-metallic antiferromagnets

B and B' in $La_2BB'O_6$ can be an any pair from the 29 transition metal elements. Therefore, there are a large number of $C_2^{29}=406$ combinations, i.e., 406 possible compounds here. In the first stage of our search for the HM-AFMs, we used the FLAPW method to calculate the self-consistent electronic structure of all 406 $La_2BB'O_6$ compounds in the ideal cubic $Fm\bar{3}m$ structure, as shown in Fig. 1(a), with fixed lattice constant $a\sim7.90$ Å. Fortunately, we found seven B and B' pairs which would make $La_2BB'O_6$ compounds HM-AFM, namely, VCu, VTc, NiMo, NiW, CoMn, CoTc, and CoRe. Furthermore, only two of these seven pairs (VCu and CoMn) were predicted before by Pickett.[15]

TABLE I. Calculated physical properties of La_2VTcO_6 in the optimized [111] stacked structure. The space group of the optimized structure is reduced from the initial $Fm\bar{3}m$ to $I4/mmm$. E_t denotes the total energy. The results obtained using GGA+U are in brackets.

Space group	$I4/mmm$	
Magnetic state	FM	AFM
a (Å)	5.566	5.585
c (Å)	7.882	7.900
c/a	1.416	1.415
V (Å^3/f.u.)	122.08	123.21
$m_{V(\mu_B)}$	0.109	−1.350(−1.800)
$m_{Tc}(\mu_B)$	0.319	1.142 (1.528)
$m_t(\mu_B)$	0.633	0.0 (0.0)
$N(E_F)$ ↑	3.20	0.0 (0.0)
(states/eV/f.u.) ↓	2.79	3.91 (1.71)
gap (eV) ↑		0.596 (1.161)
$\Delta E^{AF\text{-}FM}$ (meV/f.u.)	−297.2	
E_t (meV/f.u.)	297.2	0.0

To see whether or not the HM-AFM state in these seven compounds is magnetically stable, we performed FM electronic structure calculations. Unfortunately, we found that the total energy of the HM-AFM state in La_2NiMoO_6, La_2NiWO_6, La_2CoMnO_6, La_2CoTcO_6, and La_2CoReO_6 was substantially higher than that of the FM state, by 0.135, 0.105, 0.766, 0.279, and 0.205 eV/f.u., respectively. This suggests that the HM-AFM state in these five compounds is not stable against ferromagnetism and hence we will not consider them further. In fact, La_2CoMnO_6 was predicted earlier to prefer the FM state.[15,39] For the remaining two HM-AFM candidates, namely, La_2VCuO_6 and La_2VTcO_6 HM-AFM, we further performed full structural optimizations with both the FM and AFM states as the initial state. We found that their symmetry was reduced slightly to the tetragonal $I4/mmm$ from the cubic $Fm\bar{3}m$. Encouragingly, we found that the HM-AFM state remains to be stable for both compounds. Furthermore, the AFM state in La_2VTcO_6 is much lower in total energy than the FM state, by 297 meV/f.u. (see Table I). The huge energy difference between the AFM and FM states in La_2VTcO_6 suggests that the HM-AFM state may be stable even at room temperature. Our nonmagnetic (NM) full structural optimization calculations show that the NM state in La_2VTcO_6 is only slightly above the FM state, by 3.3 meV/f.u. In contrast, the total energy difference be-

TABLE II. Calculated physical properties of La_2VCuO_6 in the optimized [111] stacked structure. The space group of the optimized structure is reduced from the initial $Fm\bar{3}m$ to $I4/mmm$. The results obtained using GGA+U are in brackets.

Space group	$I4/mmm$	
Magnetic state	FM	AFM
a (Å)	5.532	5.540
c (Å)	7.836	7.820
c/a	1.417	1.412
V (Å^3/f.u.)	119.89	119.99
$m_{V(\mu_B)}$	0.313	−0.367(−0.542)
$m_{Cu}(\mu_B)$	0.280	0.301 (0.403)
$m_t(\mu_B)$	0.757	0.0 (0.0)
$N(E_F)\uparrow$	4.98	0.0 (0.0)
(states/eV/f.u.) $\downarrow$	2.48	7.18 (6.35)
gap (eV) $\uparrow$		0.265 (0.931)
$\Delta E^{AF\text{-}FM}$ (meV/f.u.)	−6.7	
E_t (meV/f.u.)	191.0	184.3

TABLE III. Calculated physical properties of La_2VCuO_6 and La_2VTcO_6 in the optimized $P4/mmm$ [001] stacked structure. The space group remains to be $P4/mmm$. No matter whether the initial state is FM or AFM, the converged final state of La_2VCuO_6 is always ferromagnetic while that of La_2VTcO_6 is always ferrimagnetic (FiM).

Compound	La_2VCuO_6	La_2VTcO_6
Magnetic state	FM	FiM
a (Å)	3.826	3.980
c (Å)	8.118	7.806
c/a	2.122	1.961
V (Å^3/f.u.)	118.82	123.64
$m_{V(\mu_B)}$	0.731	1.417
$m_{Cu}(\mu_B)$	0.016	
$m_{Tc}(\mu_B)$		−1.054
$m_t(\mu_B)$	0.891	−0.221
$N(E_F)\uparrow$	2.84	4.18
(states/eV/f.u.) $\downarrow$	0.86	1.03
E_t (meV/f.u.)	0.0	311.5

tween the AFM and FM states in La_2VCuO_6 is rather small (−6.7 meV/f.u.) (see Table II).

To form the AFM configuration, as mentioned before, BO_3 and $B'O_3$ octahedra $La_2BB'O_6$ can also be stacked in the [001] direction, resulting in the $P4/mmm$ tetragonal structure. In order to examine whether the stacking orientation would affect the magnetic property and the structural stability in these two compounds, La_2VCuO_6 and La_2VTcO_6, we further considered the [001] stacked structure ($P4/mmm$), as shown in Fig. 1(b). We performed full structural optimization calculations starting with both the FM and AFM states in the [001] stacked structure. For La_2VTcO_6, both the FM and AFM initial states converged to the ferrimagnetic (FiM) state during the self-consistent process (Table III). However, the total energy of the FiM [001] stacked structure of La_2VTcO_6 is much higher than the HM-AFM [111] stacked structure, by 311 meV/f.u. (see Tables I and III). Therefore, La_2VTcO_6 in the HM-AFM [111] stacked structure was found to be stable. For La_2VCuO_6, both the FM and AFM initial states converged to the ferromagnetic state during the self-consistent process (Table III). Unfortunately, the FM metallic state in the [001] stacked structure was lower in total energy than the HM-AFM state in the [111] stacked structure (see Tables II and III). This indicates that for La_2VCuO_6, the HM-AFM state in the [111] stacked structure is unstable or metastable. Our NM full structural optimization calculations show that the NM state in the [001] stacked structure in La_2VCuO_6 is higher in total energy than the FM state by 83.5 meV/f.u.

B. Electronic and magnetic properties

The calculated physical properties of La_2VTcO_6 and La_2VCuO_6 in the fully optimized [111] stacked structure are summarized in Tables I and II, respectively. The corresponding total and orbital-decomposed density of states (DOS) are displayed in Figs. 2 and 3, respectively. It is clear from Figs. 2 and 3 as well as Tables I and II that the AFM state of La_2VTcO_6 and La_2VCuO_6 in the [111] stacked structure is half-metallic with the spin-up channel being insulating and the spin-down channel being metallic. Nonetheless, some discernible differences between La_2VTcO_6 and La_2VCuO_6 exist. For example, the spin-down DOS at the Fermi level (E_F) for La_2VCuO_6 is larger (~7.18 state/eV/f.u.) than that for La_2VTcO_6(~3.91 state/eV/f.u.) (see Tables I and II).

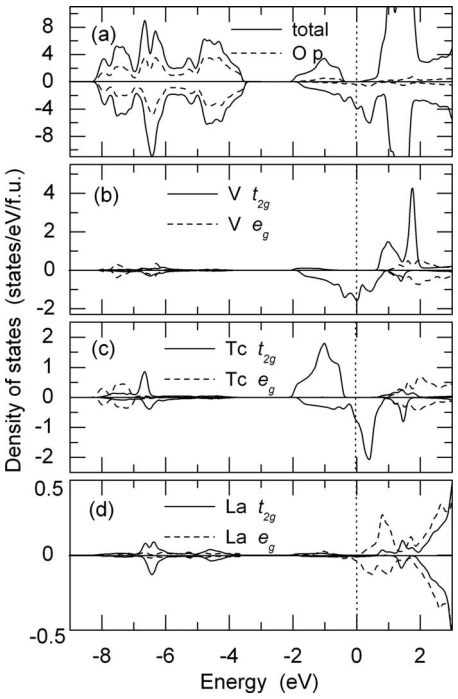

FIG. 2. Total and orbital-decomposed density of states of La_2VTcO_6 with $I4/mmm$ [111] stacked structure.

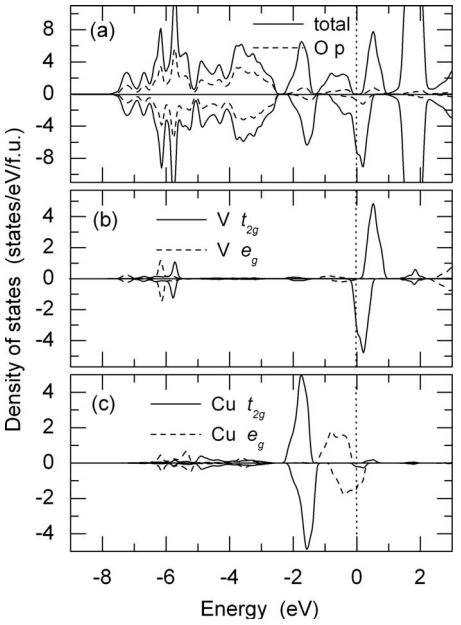

FIG. 3. Total and orbital-decomposed density of states of La_2VCuO_6 with $I4/mmm$ [111] stacked structure.

On the other hand, the insulating gap in the spin-up channel for La_2VTcO_6 is larger (~0.60 eV) than that for La_2VCuO_6(~0.26 eV). Moreover, the spin magnetic moments of the B and B' in La_2VTcO_6 are much larger (about $1.14-1.35\mu_B$/atom) than that in La_2VCuO_6.

In the ionic picture, the atoms in ordered double perovskites have the nominal valence states of $La_2^{3+}(BB')^{6+}O_6^{2-}$. Therefore, in La_2VCuO_6, the transition metal atoms B and B' can have valence configurations of $V^{4+}(3d^1)$ and $Cu^{2+}(3d^9)$, and the antiferromagnetic coupling of the spin $V^{4+}(t_{2g}^1\uparrow, S=1/2)$ and the low spin $Cu^{2+}(t_{2g}^3\uparrow t_{2g}^3\downarrow e_g^2\uparrow e_g^1\downarrow, S=1/2)$ states would give rise to an AFM state with zero total magnetic moment. Alternatively, the transition metal atoms B and B' can have valence configurations of $V^{3+}(3d^2)$ and $Cu^{3+}(3d^8)$, and the antiferromagnetic coupling of the spin $V^{3+}(t_{2g}^2\uparrow, S=1)$ with the high spin $Cu^{3+}(t_{2g}^3\uparrow t_{2g}^3\downarrow e_g^2\uparrow, S=1)$ states. Of course, in the real materials, the above simple ionic model would be modified because of hybridization between V(Cu) $3d$ and O $2p$ orbitals. The deviation from the simple ionic model is clear when considering the calculated occupation numbers of the transition metal d orbital. In the AFM state of La_2VCuO_6 in the $I4/mmm$ structure, the electron numbers are divided into $0.985e$ for spin up and $1.354e$ for spin down at the V site, and $4.613e$ for spin up and $4.312e$ for spin-down on the Cu site, giving rise to a charge configuration of $V^{2.7+}(3d^{2.3})$ and $Cu^{2.1+}(3d^{8.9})$. This is further supported by the fact that the calculated local spin magnetic moments of V and Cu are not integer numbers of 2 or 1 but less than 1.0 (see Table II). This latter fact indicates that V and Cu ions in La_2VCuO_6 are $V^{4+}(3d^1)$ and $Cu^{2+}(3d^9)$ in low spin states, respectively. Similarly, for La_2VTcO_6, the fact that the spin moments of the V and Tc ions are more than $1.0\mu_B$/atom (Table I) suggests that the valence configurations of V and Tc are close to $V^{3+}(3d^2)$ and $Tc^{3+}(4d^4)$, while the antiferromagnetic coupling of the high spin $V^{3+}(t_{2g}^2\uparrow, S=1)$ with the low spin $Tc^{3+}(t_{2g}^3\uparrow t_{2g}^1\downarrow, S=1)$ states, results in zero net magnetic moment. However, the calculated occupation numbers are $0.587e$ for spin-up and $1.923e$ for spin-down for V, and $2.401e$ for spin up and $1.266\ e$ for spin down for Tc, indicating the valence configurations of $V^{2.5+}(3d^{2.5})$ and $Tc^{3.3+}(4d^{3.7})$.

The DOS spectra for La_2VTcO_6 in the $I4/mmm$ structure displayed in Fig. 2 show that the O $2p$ orbital dominates the lower valence band between 3.5 and 8.3 eV below E_F, and the spin up Tc t_{2g} dominates the upper valence band between 0.4 and 2.0 eV below E_F. For the spin-down band, Tc t_{2g} and V t_{2g} orbitals hybridize strongly to form the part of the conduction band between −2.0 eV and 1.0 eV (Fig. 2). Also, for the spin-up band, V t_{2g}, Tc e_g, and V e_g orbitals mix substantially to dominate the upper conduction band about 0.6 eV above E_F. Nonetheless, Fig. 2 also shows that the lower valence band contains rather significant contributions from transition metal V and Tc d orbitals. This rather strong hybridization between O p and V and Tc d pushes the e_g dominant band above the t_{2g} dominant band, resulting in the crystal field splitting of the t_{2g} and e_g of about 2.0 and 1.6 eV for the VO_6 and TcO_6 octahedra, respectively. This kind of Bd-O p-$B'd\sigma$ bonding is the well-known superexchange coupling among the B and B' ions which is the cause giving rise to the AFM exchange interaction between B and B' ions. This is similar to the conventional superexchange in the AFM insulators (e.g., NiO) where a large superexchange energy gap between the majority (minority) and minority (majority) d orbitals for the transition metal ions also exists.

In La_2VTcO_6, the energy of majority spin V t_{2g} and minority spin Tc t_{2g} orbitals are very close to each other. This causes a strong hybridization between the majority spin V t_{2g} and minority spin Tc t_{2g} orbitals via O p-π orbitals which broaden the B and B' t_{2g} spin-down conduction band in the energy range of −2.0 to 1.0 eV. This hybridization also strengthens the AFM exchange coupling between the V and Tc ions. Clearly, this coupling between the V and Tc t_{2g} orbitals via O p-π orbitals allows the spin-down conduction electrons to hop freely from a V ion to the neighboring Tc ions and back to the V ion, lowering the kinetic energy of the system. This situation is similar to the double exchange mechanism[40] of the metallic ferromagnetism in the colossal magneto resistive manganites and, in fact, has been called the generalized double exchange mechanism.[17] The direct-site exchange interaction lowers the majority spin Tc t_{2g} band to below E_F and pushes the minority spin V t_{2g} band above E_F, thereby creating an insulating gap in the spin-up channel (see Fig. 2). As a result, the band gap in La_2VTcO_6 may be called an antiferromagnetic coupling gap which has the dominant contributions from both the superexchange and the generalized double exchange mechanisms (see Refs. 41 and 42 for the detailed analysis of these two mechanisms in the doped ferromagnetic manganites). The origin of the half-metallicity is essentially similar to that of the HM ferromagnetic double perovskites (e.g., Sr_2FeMoO_6), i.e., the hybridization of Bt_{2g}-O$(2p_\pi)$-$B't_{2g}$, as discussed in Refs. 8 and 43. Hence, according to this viewpoint, it could be inferred that the antiferromagnetic transition temperature T_N in the HM-AFMs would be on the same order of magnitude as that in

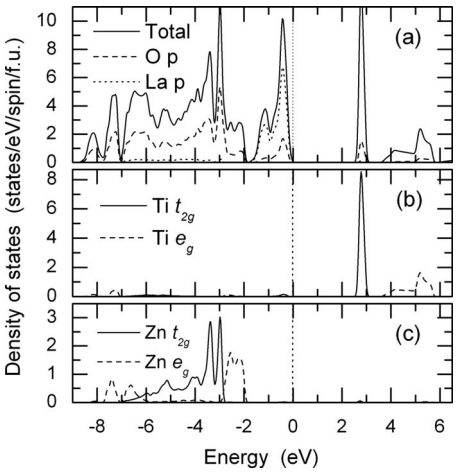

FIG. 4. Total and orbital-decomposed density of states of La_2TiZnO_6 with $I4/mmm$ [111] stacked structure.

Sr_2FeMoO_6(T_c=419 K),[3] i.e., being above room temperature.

Inspection of Figs. 2 and 3 reveals that there are some discernible differences in the electronic structure between La_2VCuO_6 and La_2VTcO_6. For example, the contribution of Tc 4d orbital to the O 2p dominant lower valence band is more pronounced than that of Cu 3d orbital, indicating the stronger Tc 4d-O 2p bonding in La_2VTcO_6. This may be expected because Tc 4d orbital is significantly more extended than Cu 3d orbital. Also, the V 3d dominant band around E_F in La_2VCuO_6 is substantially narrower than that in La_2VTcO_6 [see Figs. 2(b) and 3(b)]. This gives rise to a larger spin-down DOS at E_F for La_2VCuO_6 (7.18 state/eV/f.u.) than that for La_2VTcO_6 (3.91 state/eV/f.u.), but a smaller insulating gap in the spin-up channel for La_2VCuO_6 (0.26 eV) than that for La_2VTcO_6 (0.60 eV). Another interesting difference is that the insulating gap in La_2VCuO_6 is between the occupied Cu e_g and unoccupied V t_{2g} states in the spin-up (majority spin) bands (Fig. 3) while it is between the occupied Tc t_{2g} and unoccupied La e_g states in the spin-up channel (Fig. 2). Finally, the hybridization of V t_{2g} and Tc t_{2g} in La_2VTcO_6 is clearly stronger than that of V t_{2g} and Cu e_g in La_2VCuO_6. This could be a main reason why the AFM state in La_2VTcO_6 is energetically more stable than that in La_2VCuO_6 (see the $\Delta E^{\text{AF-FM}}$ in Tables I and II).

According to the simple ionic picture, many of the 406 compounds considered here could have been a HM-AFM. For example, the Cr and Mo atoms in La_2CrMoO_6 may have valence configurations of $Cr^{4+}(3d^2)$ and $Mo^{2+}(4d^8)$, respectively, thereby resulting in a HM-AFM. Another example is La_2TiZnO_6 where the Ti and Zn could have $Ti^{3+}(3d^1)$ and $Zn^{3+}(3d^9)$ configurations, respectively. To help understand why half-metallic antiferromagnets are very rare, we display the calculated band structure of La_2TiZnO_6 in Fig. 4. We noticed that for La_2TiZnO_6 in the fully optimized [111] stacked structure, both FM and AFM initial states were converged to the insulating nonmagnetic state. Due to hybridization between the orbitals of Ti(Zn) 3d, O 2p, and La 5p, the calculated valence configuration of La_2TiZnO_6 are $Ti^{2.77+}(3d^{1.23})$ and $Zn^{2.40+}(3d^{9.60})$. Furthermore, quite unexpectedly, the lowest conduction band is La 5p orbital dominant rather than of Ti 3d orbital character. In short, although based on the ionic picture, many double perovskite oxides are expected to be a HM-AFM, they are not in reality due to effects of, e.g., hybridization of metal d orbitals and O p orbitals, structural relaxation, and also rare earth s/p valence electrons. Therefore, *ab initio* calculations are essential in searching for real HM-AFM materials.

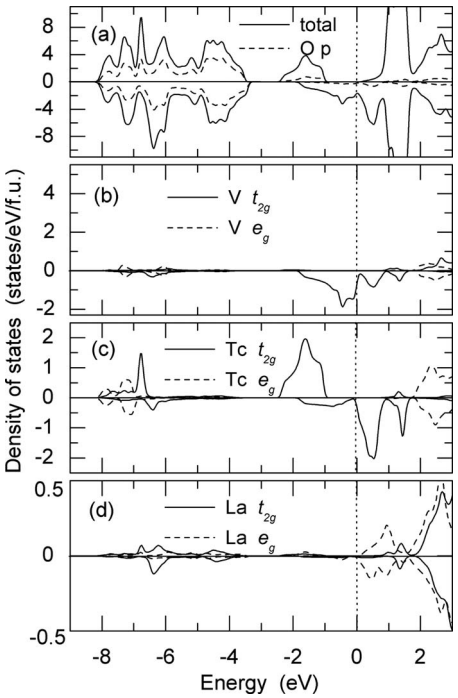

FIG. 5. Total and orbital-decomposed density of states of La_2VTcO_6 with $I4/mmm$ [111] stacked structure from the GGA+U calculations.

C. Effects of on-site Coulomb interactions

Electron-electron correlation is known to be rather strong in transition metal oxides. Thus a better description of the electronic structure of these materials is to include the electron correlations between d electrons. By utilizing the orbital-dependent potential, the LDA(GGA)+U method provides a simple way that incorporates correlations beyond the LDA and GGA.[34,35] We have therefore performed the GGA+U calculations for La_2VTcO_6 and La_2VCuO_6 in order to see whether or not the HM-AFM would be destroyed by the on-site Coulomb interaction. In these calculations, the parameters for GGA+U are U=4.0 eV and J=0.87 eV for V 3d and U=2.0 eV and J=0.87 eV for Tc 4d or Cu 3d. The calculated electronic and magnetic properties are listed in Tables I and II and the total and orbital-decomposed DOS spectra are displayed in Figs. 5 and 6. Importantly, the GGA+U calculations yield an electronic structure for La_2VTcO_6 and La_2VCuO_6 that is not qualitatively different from the GGA calculations (Figs. 2 and 3). In particular, as for the GGA calculations, the GGA+U calculations also give rise to a HM-AFM electronic structure for La_2VTcO_6 and La_2VCuO_6. Interestingly, the only pronounced changes from the GGA+U calculations are the increase in the spin-up in-

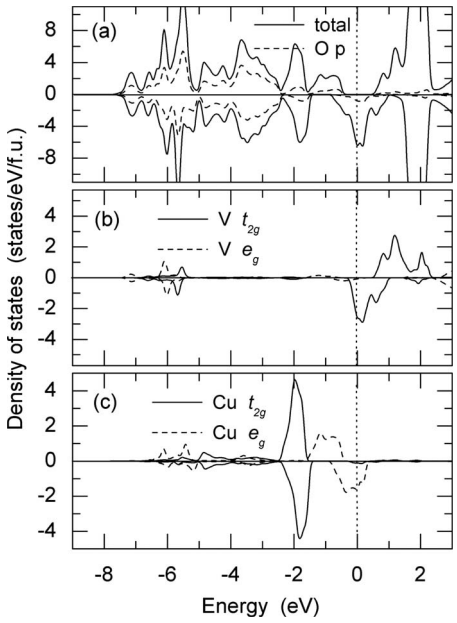

FIG. 6. Total and orbital-decomposed density of states of La_2VCuO_6 with $I4/mmm$ [111] stacked structure from the GGA+U calculations.

sulating gap from 0.596 to 1.161 eV and the enhancement of the local magnetic moments from 1.350 (1.142) to 1.800 (1.528) for V (Tc) (see Table I). Similar results from GGA and GGA+U calculations of La_2VCuO_6 are listed in Table II. These changes may be expected. Taking on-site Coulomb interaction into account would lower the related occupied d band and raise the related unoccupied d band,[34,36] thereby increasing the insulating gap. Furthermore, this would also enhance the localization of the related d orbitals and hence increase the local magnetic moments on the related transition metal sites.[36,38]

D. Structural properties

The theoretical lattice constants and atomic positions of La_2VTcO_6 and La_2VCuO_6 are listed in Tables I–V. For $La_2BB'O_6$ in the ideal cubic perovskite with [111] stacking ($Fm\bar{3}m$), the B and B' order in the NaCl configuration, and are described by a fcc lattice with lattice constant $2a'$ (a' means the length of the O-B-O bond in the single perovskite). Each $B(B')$ is coordinated by 6 $B'(B)$ so that there are 6 B-O-B' bonds per unit cell where the lengths of B-O and B'-O bonds are equal. Thus, there is only one kind of O atoms. After full structural optimization, the cubic $Fm\bar{3}m$ structure is reduced to the tetragonal $I4/mmm$ structure with two inequivalent kinds of O atoms (Tables IV and V). There are two O_1 atoms sitting above and below the B and B' atoms along the z axis, and the other four O_2 atoms sitting on the same plane as the B and B' atoms. [see Fig. 1(a) as well as Tables IV and V]. However, this symmetry reduction is rather minor since the shape (i.e., the c/a ratio being very close to the ideal value of $\sqrt{2}$) of the unit cell for these two compounds hardly changes after the structural optimization (Tables I and II). Furthermore, in La_2VTcO_6, the angle of the B-O-B' bond remains to be 180° after full structural optimization, and this may be due to the fact that V and Tc have rather similar atomic radii of 2.82 and 2.84 a.u., respectively.[44] Nonetheless, the contraction (expansion) of the V-O_2 (Tc-O_2) bond in La_2VTcO_6 is discernible, being about 1.88(1.84)%. Perhaps due to the fact that the atomic

TABLE IV. Calculated structural parameters of La_2VTcO_6.

Space group	$I4/mmm$		$P4/mmm$
Magnetic state	FM	AFM	FiM
$B(x,y,z)$	(0,0,0)	(0,0,0)	(0,0,0)
$B'(x,y,z)$	$(0,0,\frac{1}{2})$	$(0,0,\frac{1}{2})$	$(0,0,\frac{1}{2})$
O_1 x	0	0	0
y	0	0	0
z	0.7568	0.7547	0.2434
O_2 x	0.2568	0.2547	0
y	0.7432	0.7453	$\frac{1}{2}$
z	$\frac{1}{2}$	$\frac{1}{2}$	$\frac{1}{2}$
$O_3(x,y,z)$			$(\frac{1}{2},0,0)$
La x	$\frac{1}{2}$	$\frac{1}{2}$	$\frac{1}{2}$
y	0	0	$\frac{1}{2}$
z	$\frac{1}{4}$	$\frac{1}{4}$	0.2460
$B-O_1$ (Å)	1.917	1.938	1.900
$B'-O_1$ (Å)	2.024	2.012	2.003
$B-O_2$ (Å)	1.914	1.938	
$B'-O_2$ (Å)	2.021	2.011	1.990
$B-O_3$ (Å)			1.990

TABLE V. Calculated structural parameters of La_2VCuO_6.

Space group	$I4/mmm$		$P4/mmm$
Magnetic state	FM	AFM	FiM
$B(x,y,z)$	(0,0,0)	(0,0,0)	(0,0,0)
$B'(x,y,z)$	$(0,0,\frac{1}{2})$	$(0,0,\frac{1}{2})$	$(0,0,\frac{1}{2})$
O_1 x	0	0	0
y	0	0	0
z	0.7596	0.7595	0.2357
O_2 x	0.2595	0.2595	0
y	0.7405	0.7405	$\frac{1}{2}$
z	$\frac{1}{2}$	$\frac{1}{2}$	$\frac{1}{2}$
$O_3(x,y,z)$			$(\frac{1}{2},0,0)$
La x	$\frac{1}{2}$	$\frac{1}{2}$	$\frac{1}{2}$
y	0	0	$\frac{1}{2}$
z	$\frac{1}{4}$	$\frac{1}{4}$	0.2719
$B-O_1$ (Å)	1.884	1.881	1.914
$B'-O_1$ (Å)	2.034	2.029	2.146
$B-O_2$ (Å)	1.882	1.884	
$B'-O_2$ (Å)	2.030	2.033	1.913
$B-O_3$ (Å)			1.913

radius of Cu (2.67 a.u.) is smaller than that of Tc (also V), the theoretical lattice constants of La_2VCuO_6 are smaller than that of La_2VTcO_6 (Tables I and II). Also, for La_2VCuO_6, the contraction (expansion) of the V-O_2 (Cu-O_2) bond is rather large, being about 4.62(2.95)%.

In comparison, in the ideal [001] stacked tetragonal perovskite ($P4/mmm$), each B atom is coordinated by 4 B and 2 B' sites, and vice versa. Therefore, for each unit cell, there are 2 B-O-B', 2 B'-O-B', and 2 B-O-B bonds, and hence there are three different kinds of nonequivalent O sites (Tables IV and V). After full structural optimization, its symmetry remains intact (i.e., $P4/mmm$). However, both the lattice constants and the length of $B(B')$-O bonds change significantly after the structural optimization (see Tables III–V). In particular, in La_2VCuO_6, the planar lattice constant a is reduced by ~3.1%, while the vertical lattice constant c is expanded by ~2.7%. The contraction (expansion) of the V-O_1 (Cu-O_1) bond is about 3.10(8.63)%. The lattice constant changes of La_2VTcO_6 are, however, smaller (within 1.2%), and the contraction (expansion) of the V-O_1 (Tc-O_1) bond is about 3.79(1.40)%.

IV. CONCLUSIONS

In conclusion, in order to search for new half-metallic antiferromagnetic materials within the family of double perovskites, we have performed the self-consistent FLAPW electronic structure calculations for double perovskites $La_2BB'O_6$ in the [111] stacked structure with all possible B and B' pairs from all 3d, 4d, and 5d transition metals with 406 perovskites in total. Fortunately, we find two HM-AFMs, namely La_2VCuO_6 and La_2VTcO_6 in the [111] stacked structure. Further PAW full structural optimization calculations for these two compounds in both the [111] and [001] stacked structures show that La_2VTcO_6 in the [111] stacked structure is the stable structure, though La_2VCuO_6 in the [111] stacked structure is metastable. The FM state of La_2VCuO_6 in the [001] stacked structure is the stable state. Furthermore, the found HM-AFM state in La_2VTcO_6 and La_2VCuO_6 survives in the GGA+U electronic structure calculations. In particular, the huge energy difference between the HM-AFM La_2VTcO_6 with the [111] stacked structure and the FiM La_2VTcO_6 with the [001] stacked structure implies that La_2VTcO_6 with the [111] stacked structure is a promising candidate for a HM-AFM. We hope that our interesting predictions will encourage further experimental searches for the half-metallic antiferromagnets.

ACKNOWLEDGMENTS

The authors gratefully acknowledge financial supports from the National Science Council and also NCTS of Taiwan. The authors also thank the National Center for High-performance Computing of Taiwan for CPU time.

*kant@ntnu.edu.tw
†gyguo@phys.ntu.edu.tw

[1] R. A. de Groot, F. M. Müeller, P. G. van Engen, and K. H. J. Buschow, Phys. Rev. Lett. **50**, 2024 (1983).
[2] J.-H. Park, E. Vescovo, H.-J. Kim, C. Kwon, R. Ramesh, and T. Venkatesan, Nature (London) **392**, 794 (1998).
[3] K.-I. Kobayashi, T. Kimura, H. Sawada, K. Terakura, and Y. Tokura, Nature (London) **395**, 677 (1998).
[4] W. E. Pickett and J. S. Moodera, Phys. Today **54** (5), 39 (2001).
[5] H.-T. Jeng and G. Y. Guo, Phys. Rev. B **65**, 094429 (2002).
[6] K. Schwarz, J. Phys. F: Met. Phys. **16**, L211 (1986).
[7] W. E. Pickett and D. J. Singh, Phys. Rev. B **53**, 1146 (1996).
[8] H.-T. Jeng and G. Y. Guo, Phys. Rev. B **67**, 094438 (2003).
[9] M. S. Park, S. K. Kwon, S. J. Youn, and B. I. Min, Phys. Rev. B **59**, 10018 (1999).
[10] M. Shirai, T. Ogawa, I. Kitagawa, and N. Suzuki, J. Magn. Magn. Mater. **177-181**, 1383 (1998).
[11] J. H. Park, S. K. Kwon, and B. I. Min, Physica B **281-282**, 703 (2000).
[12] H. van Leuken and R. A. de Groot, Phys. Rev. Lett. **74**, 1171 (1995).
[13] S. Wurmehl, H. C. Kandpal, G. H. Fecher, and C. Felser, J. Phys.: Condens. Matter **18**, 6171 (2006).
[14] I. Galanakis, K. Özdogan, E. Sasioglu, and B. Aktas, Phys. Rev. B **75**, 172405 (2007).
[15] W. E. Pickett, Phys. Rev. B **57**, 10613 (1998).
[16] J. H. Park, S. K. Kwon, and B. I. Min, Phys. Rev. B **65**, 174401 (2002).
[17] Y. K. Wang and G. Y. Guo, Phys. Rev. B **73**, 064424 (2006).
[18] M. S. Park and B. I. Min, Phys. Rev. B **71**, 052405 (2005).
[19] M. S. Park, S. K. Kwon, and B. I. Min, Phys. Rev. B **64**, 100403(R) (2001).
[20] D. Ködderitzsch, W. Hergert, Z. Szotek, and W. M. Temmerman, Phys. Rev. B **68**, 125114 (2003).
[21] I. Galanakis, K. Özdogan, E. Sasioglu, and B. Aktas, Phys. Rev. B **75**, 092407 (2007).
[22] H. Akai and M. Ogura, Phys. Rev. Lett. **97**, 026401 (2006).
[23] L. Bergqvist and P. H. Dederichs, J. Phys.: Condens. Matter **19**, 216220 (2007).
[24] W. E. Pickett, Phys. Rev. Lett. **77**, 3185 (1996).
[25] K. Ueda, H. Tabata, and T. Kawai, Science **280**, 1064 (1998).
[26] P. Hohenberg and W. Kohn, Phys. Rev. **136**, B864 (1964); W. Kohn and L. J. Sham, *ibid.* **140**, A1133 (1965).
[27] J. P. Perdew, K. Burke, and M. Ernzerhof, Phys. Rev. Lett. **77**, 3865 (1996).
[28] P. E. Blöchl, Phys. Rev. B **50**, 17953 (1994); G. Kresse and D. Joubert, *ibid.* **59**, 1758 (1999).
[29] G. Kresse and J. Hafner, Phys. Rev. B **48**, 13115 (1993); G. Kresse and J. Furthmüller, Comput. Mater. Sci. **6**, 15 (1996); Phys. Rev. B **54**, 11169 (1996).
[30] O. K. Andersen, Phys. Rev. B **12**, 3060 (1975).
[31] D. D. Koelling and G. O. Arbman, J. Phys. F: Met. Phys. **5**, 2041 (1975).
[32] P. Blaha, K. Schwarz, G. K. H. Madsen, D. Kvasnicka, and J. Luitz, WIEN2K, An Augmented Plane Wave Local Orbitals Program for Calculating Crystal Properties, Techn. University,

Wien, Austria, 2002.
[33] P. E. Blöchl, O. Jepsen, and O. K. Andersen, Phys. Rev. B **49**, 16223 (1994).
[34] V. I. Anisimov, J. Zaanen, and O. K. Andersen, Phys. Rev. B **44**, 943 (1991).
[35] A. I. Liechtenstein, V. I. Anisimov, and J. Zaanen, Phys. Rev. B **52**, R5467 (1995).
[36] V. I. Anisimov, F. Aryasetiawan, and A. I. Lichtenstein, J. Phys.: Condens. Matter **9**, 767 (1997).
[37] X. Jiang and G. Y. Guo, Phys. Rev. B **70**, 035110 (2004).
[38] H.-T. Jeng, G. Y. Guo, and D. J. Huang, Phys. Rev. Lett. **93**, 156403 (2004).
[39] R. I. Dass and J. B. Goodenough, Phys. Rev. B **67**, 014401 (2003).
[40] C. Zener, Phys. Rev. **82**, 403 (1951).
[41] I. V. Solovyev and K. Terakura, Phys. Rev. Lett. **82**, 2959 (1999).
[42] I. V. Solovyev and K. Terakura, in *Electronic Structure and Magnetism of Complex Materials*, edited by D. J. Singh and D. A. Papaconstantopoulos (Springer-Verlag, Berlin, 2003).
[43] H. Wu, Phys. Rev. B **64**, 125126 (2001).
[44] H. L. Skriver, *The LMTO Method* (Springer-Verlag, Berlin, 1984), Table 10.1.